UCLA-ENG--8626
DE86 012968

UCLA-ENG-8626
PPG-966

Papers Presented at the Second International Fusion Reactor Materials Conference - Chicago, Ill.

Jamal Alhajji, Philip Chou, Nasr Ghoniem, [illegible]
and Rodger Martin

April 14-19, 1986

EAB

DISCLAIMER

Comprehensive Modeling of Creep Fracture by Grain Boundary Cavitation in Irradiated Structural Alloys*

by

J.N. Al-Hajji** and Nasr M. Ghoniem

**Mechanical Engineering Department,
Kuwait University,
P.O. Box 5969, Kuwait

March 1986

*This work was supported by the U.S. Department of Energy, Office of Fusion Energy, Grant #DE-FG03-84ER52110, with UCLA.

CONTENTS

FIGURES

COMPREHENSIVE MODELING OF CREEP FRACTURE BY GRAIN BOUNDARY CAVITATION IN IRRADIATED STRUCTURAL ALLOYS

J. N. Al-Hajji and Nasr M. Ghoniem

ABSTRACT

The present model describes high-temperature helium embrittlement as a sequence of four inter-linked steps. First helium clustering in the matrix is described by the conventional rate theory. This is then coupled to rate equations for the transport of single helium atoms to grain boundaries in the second phase. The third step addresses the influence of helium and stress on the nucleation of cavities at GBs, with particular emphasis on the role that precipitates and triple-point junctions play in the nucleation process. The last phase of this work is concerned with various growth modes of grain boundary cavities which lead to fracture by the inter-linkage of equally spaced GB cavities. The model proposes a new explanation of the creep rupture behavior of martensitic steels as opposed to austenitic steels. Vacancy source limitation at GBs resulting from dislocation interactions is identified as the primary reason for the retarded growth of GB cavities in martensitics.

1. Introduction

Fracture of alloys at high temperature is now widely recognized to result from the influence of the applied stress on the nucleation and growth of grain boundary (GB) cavities. Several investigators have proposed theoretical models to describe the mechanistic physical process underlying this important phenomenon. For convenience, theories in this area have tended to address either the nucleation phase of cavities (e.g., refs. [1-4]), or the growth mechanisms controlling the rapid expansion of GB cavities under the influence of an applied stress at high temperature (e.g., refs. [5-8]). During irradiation in a neutron environment, other physical processes must be considered. Energetic neutrons displace lattice atoms creating Frenkel pairs, and also produce substantial amounts of hydrogen and helium. Point-defect diffusion enhances non-equilibrium rate processes governing microstructure evolution; hence, the nucleation and growth phases of GB cavities. On the other hand, helium, which has low solubility in most metals, tends to segregate within the matrix before reaching grain boundaries.

A host of interesting questions arise in trying to understand the relative roles on the fracture process of temperature, stress, displacement damage, helium production, as well as the specific variables inherent to the structure of the material itself. The present model is an effort to unravel the actions of some of these mechanisms and to explain, by comparison with experimental data, the differences in the behavior of austenitic and martensitic alloys. First we summarize our work in two areas: helium

transport to GBs and GB cavity nucleation under irradiation. Next, delineation of GB cavity growth and fracture is presented as a part of an integrated model of high-temperature fracture under irradiation. Finally, results and conclusions are given in Section 4.

2. Helium Transport and GB Cavity Nucleation

A rate theory formalism has been recently developed by Ghoniem, Al-Hajji and Kalletta [9] to analyze the problem of helium clustering in the matrix and its transport to GBs. Furthermore, the problem of GB cavity nucleation under the combined influence of helium generation and an applied stress has been presented in another publication [10]. Fundamental rate equations are developed and numerically solved for a selected number of species which describe helium clustering and transport to grain boundaries. Conservation equations are solved for single vacancies, single interstitials, interstitial helium atoms, substitutional helium, relevant helium-vacancy clusters which lead to the direct (spontaneous) nucleation of helium-filled cavities, the concentration of matrix cavities, the average number of helium atoms in a cavity, the average radius of various matrix cavities, and finally the rate of transport of helium atoms to the grain boundary.

The work reveals interesting facets of helium behavior in the presence of Frenkel pairs resulting from displacement damage. If the helium production rate is significant, as is expected in fusion reactor first-wall materials, vacancies are immobilized in the matrix which leads to a slow mode of growth for matrix cavities. This effect, coupled with a high rate of gas

re-solution from cavities, is shown to result in continuous (dynamic) nucleation throughout irradiation.

The matrix cavity structure can be characterized by a uniform population of small cavities, with the exception of those associated with precipitates. During early irradiation, helium gas is trapped in small vacancy clusters; however a significant fraction ends up at the GBs. The nucleation and subsequent growth of matrix cavities reduces the chances of helium migrating to the grain boundary because newly introduced helium can now be absorbed at matrix cavities and precipitates. Nevertheless, it is found that a small amount of helium is bound to reach the grain boundary. To reduce this harmful amount of helium, trapping in the matrix must be further enhanced through the introduction of a uniform concentration of precipitates in the matrix, as is experimentally observed [11,12]. The only real limitation on this method of alloy tailoring is the concomitant reduction in ductility.

The nucleation of GB cavities is treated as a consequence of a combination of applied stress and helium escaping from the matrix, as determined by the previous step [10]. A modification to classical nucleation theory to account for site occupancy at triple-point junctions and GB precipitates leads to the following equation [10]:

$$\dot{C} = (C_{max} - C)\left[\left(\frac{\pi}{12F_v\gamma_s^3 kT}\right)^{\frac{1}{2}} \sigma_L^2 D_b \delta \exp\left(-\frac{\Delta G_c}{KT}\right)\right] \quad , \qquad (1)$$

where C_{max} is the maximum number of available nucleation sites per unit area of GBs, F_v is the volumetric shape factor, γ_s is the cavity surface energy, k is Boltzmann's constant, T is the temperature, Δ is the boundary thickness,

σ_L is the local stress, D_b is the grain boundary diffusivity, and ΔG_c is the change in free energy resulting from the introduction of cavities on a stressed boundary.

Local stress loading and unloading is phenomenologically modeled at triple-point junctions and GB-precipitate interfaces. The resulting time-dependent stress is introduced in eq. (1), which is subsequently numerically integrated. The influence of helium on GB cavity nucleation is studied via rate theory. Appropriate hierarchial equations are simultaneously solved for the helium-induced nucleation of GB cavities. Reasonable correlation with experimental data [11] has been achieved for an effective helium migration energy close to the self-diffusion energy.

Grain boundary inclination to the principal direction of the applied stress is found to be an important parameter and it displays a great influence on the rate of cavity nucleation. It is assumed in this work that irregularities with inclinations on the order of 10 to 20 deg occur at normal boundaries. Fig. 1 shows the density of cavity nuclei for various boundary inclinations for a ferritic alloy at 600°C and a stress of 100 MPA. It could be seen that, depending on the inclination angle, available nucleation sites could be saturated during one stress loading and unloading pulse for large inclinations, or they may require a number of such repetitive pulses. This will depend on the stochastic nature of stress localization due to sliding, which is not addressed in this paper.

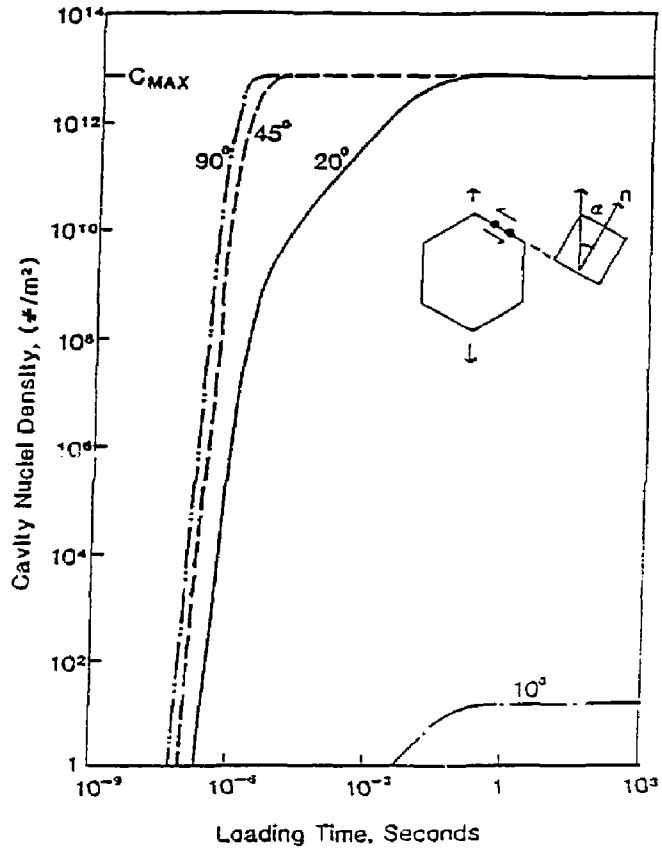

Fig. 1. Density of cavity nuclei at boundaries of various inclinations at 600°C and F_V value of 0.01 as a result of a single sliding pulse. The applied stress is 100 MPa

Helium, on the other hand, is found to lead to rapid homogeneous nucleation of cavities on the GB; the quasi-steady-state density being reached at 1 to 10 appm helium. The work shows that, consistent with experiments, irradiation-generated GB bubble densities are generally orders of magnitude greater than those observed in creep experiments in the absence of irradiation. Small amounts of total injected helium (≈ 1 appm He) may result in GB bubble densities as high as 10^9 cm^{-2}. During irradiation, it can be safely assumed that nucleation of GB cavities is rapidly achieved, and that the majority of cavity lifetime is spent in the growth regime.

3. Grain Boundary Cavity Growth and Fracture

Earlier growth models of GB cavities have assumed that the GB is essentially an inexhaustible source of vacancies that are readily available for cavities (e.g., refs. [4-7]). However, a recent review by Balluffi stresses the importance of the relationship between the boundary structure and the availability of vacancies [12]. Bollmann's [13] formal theory of crystalline interfaces demonstrates that it is always possible for a lattice dislocation to enter the boundary upon impingement. Fig. 2 shows a schematic representation of a model for the vacancy-source control by dislocations at GBs; the model is similar to that of Beere [14]. The model illustrated in fig. 2 is a general representation which includes the possibilities that lattice dislocations may enter or leave the boundary. By climbing in both the lattice and the boundary, dislocations can dictate the rate of vacancy creation within the boundary. Adopting Beere's approach, various growth

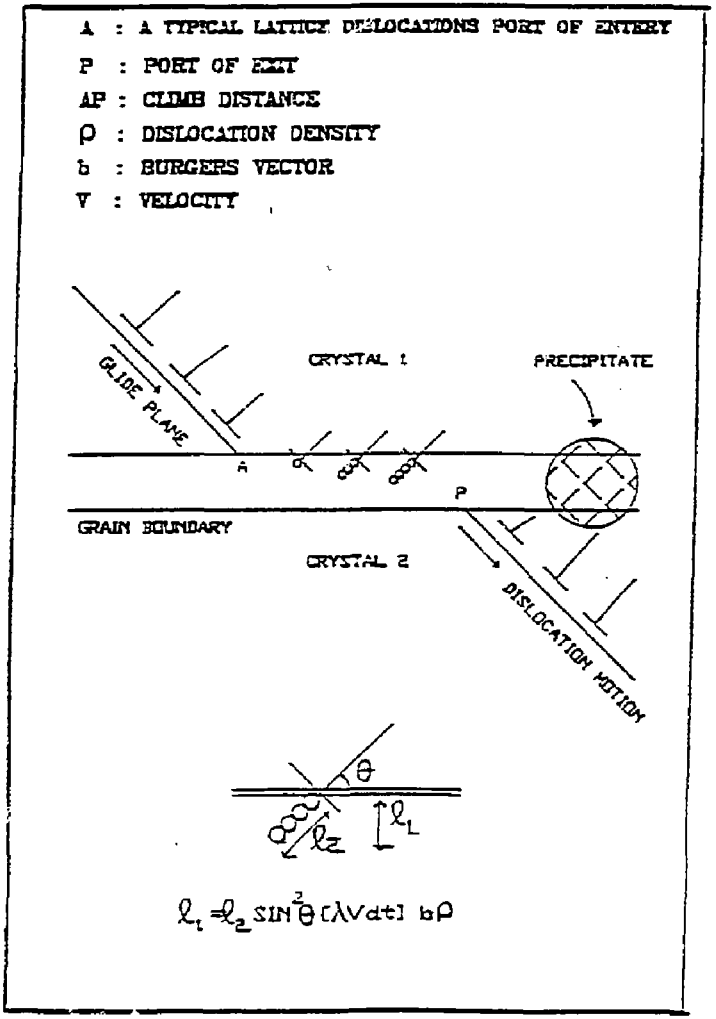

Fig. 2. A schematic illustration of lattice dislocation interactions with grain boundaries

mechanisms can be viewed as sharing mixed sequential/independent relationships. The overall volumetric cavity growth rate $\dot{V}$ is given by:

$$\dot{V} = \dot{V}_{DC} + \frac{\dot{V}_{BD}\dot{V}_{SC}}{\dot{V}_{BD} + \dot{V}_{SC}} \quad , \tag{2}$$

where $\dot{V}_{DC}$ is the growth rate due to dislocation creep, $\dot{V}_{BD}$ is the GB diffusion growth rate, and $\dot{V}_{SC}$ is the vacancy source-controlled growth rate.

Numerical calculations are performed for eq. (2), assuming that the cavity shape is lenticular. It is found that a growth instability takes place when the average cavity radius is about 60% of the average inter-cavity spacing. Experimental evidence [14] has shown that GB cavity growth rates are much smaller in ferritic/martensitic alloys as compared with austinitics. This results in significant ductile deformation in martensitics before fracture, as opposed to a much more limited ductility in austenitics. Wassilew [14] argues that twinning is the major reason for this observed discrepancy. Twin planes are assumed to supply the necessary vacancy source in austenitics, while twining does not take place in martensitics. However, this interpretation does not explain why cavities at the intersection of the few twin planes and the GBs do not grow much faster than the remainder of the population.

In this work, we consider the process of matrix dislocation entry/exit in the GB. Slip is the principal means by which plastic deformation occurs in crystalline solids. While an austenitic steel (FCC) has 12 slip systems, a martensitic alloy (BCC) would have 48. Cross-slip in BCC systems allows for much easier dislocation motion. Observed creep rates and dislocation

recovery processes are higher in martensitic alloys than in austenitic, which is commensurate with faster dislocation recovery. Since the average dislocation residence time is determined by the average distance between entry and exit planes at the GB, it is expected that this time is shorter in a martensitic alloy. This will naturally place a vacancy source limitation on the growth rate of GB cavities in martensitics. We assume in this model that, while the average GB dislocation climb distance in austenitic alloys is the GB inter-precipitate spacing, it is on the order of the GB inter-bubble spacing in martensitics.

4. Results and Conclusions

The model described in this paper is a comprehensive one involving detailed computations and various levels of approximations. Helium embrittlement is a complex phenomenon, and comparisons with experiments should still be taken cautiously. Unlike earlier attempts to explain experiments on the basis of one mechanism (e.g., refs. [15,16]), this work attempts to treat the problem in a self-consistent way. Fig. 3 compares the calculated and experimentally measured time-to-rupture for the German martensitic steel DIN 1.4914 at 600°C. The data is taken from ref. [17]. Here creep experiments were for post-irradiation conditions. The presence of helium does not drastically reduce the time-to-rupture. In fig. 4, the model and experimental values suggest a higher sensitivity to helium of the corresponding austenitic alloy (DIN 1.4970). In fig. 5, we compare calculations of time-to-rupture data of the martensitic steel (DIN 1.4914), for both unirradiated and in-reactor behavior at 600°C. The main reason for

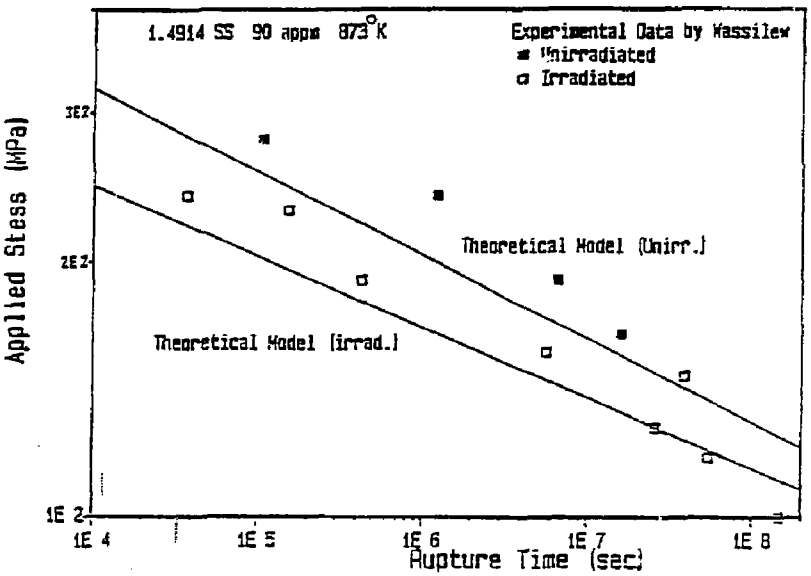

Fig. 3. A comparison of calculated and experimental time-to-rupture for the martensitic stainless steel DIN 1.4914 at 873°K (data from ref. [17])

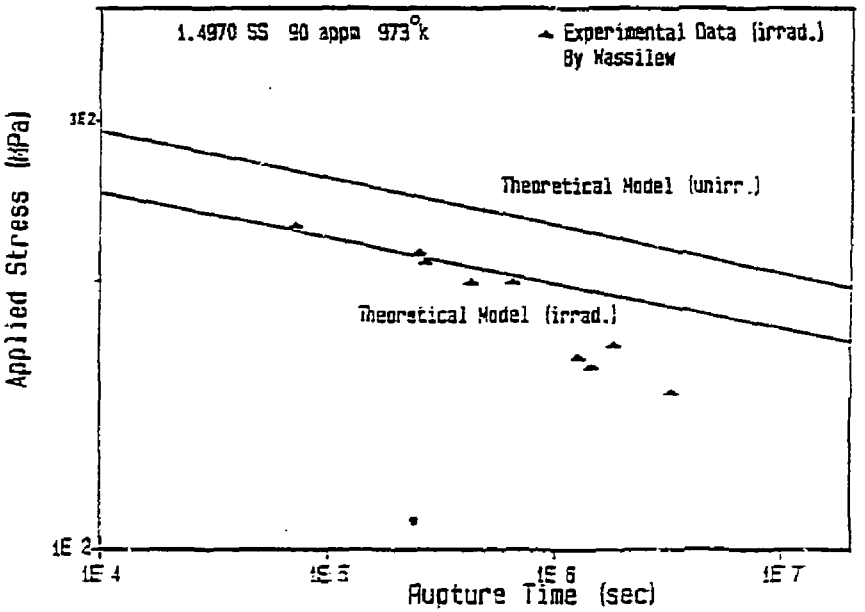

Fig. 4. A comparison of calculated and experimental time-to-rupture for the austenitic stainless steel DIN 1.4970 at 973°K (data from ref. [17])

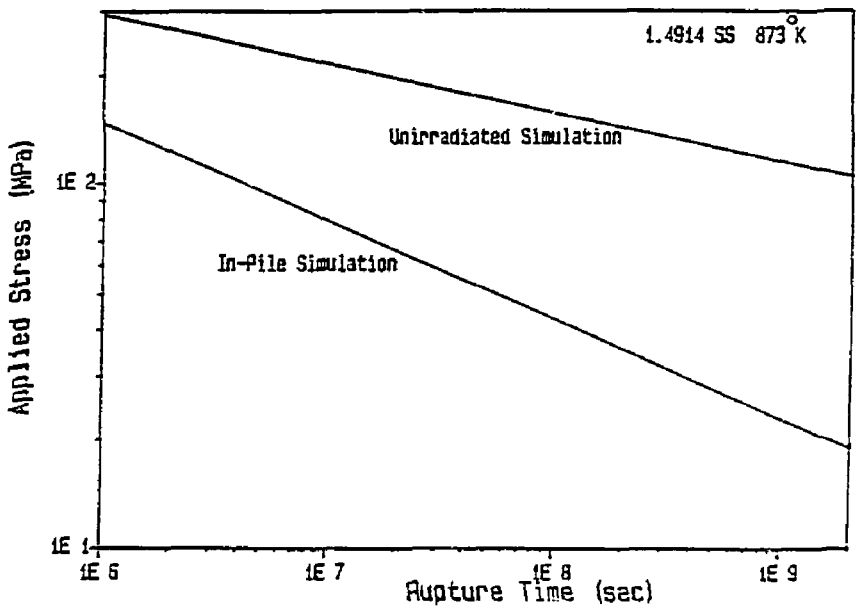

Fig. 5. A theoretical comparison of the stress dependence of the time-to-rupture of unirradiated and in-reactor tested martensitic stainless steel at 873°K

this greater sensitivity is the acceleration of in-reactor creep in martensitics only, as was recently observed by Herschbach [18].

It is concluded here that even though GB cavities in martensitic alloys are sluggish in their growth behavior, raising possibilities for the mitigation of high-temperature embrittlement, the unfortunate creep acceleration due to irradiation may still limit the upper useful design temperature limit.

Acknowledgements

Support by the Kuwait University to one of us (JNA) is appreciated. Partial Support by the U.S. Department of Energy, Office of Fusion Energy, Grant #DE-FG03-84ER52110, with UCLA is acknowledged.

References

[1] I. Servi and N.J. Grant, Trans. AIME, 191 (1951) 909.

[2] J.E. Harris, Trans. Metall. Soc. AIME, 233 (1965) 1509.

[3] R. Raj and M.F. Ashby, Acta Metall., 23 (1975) 653.

[4] A.S. Argon, I.W. Chen and C.W. Lau, in: Creep-Fatigue-Environment Interactions, Eds. R.M. Pelloux and N.S. Stoloff (AIME, N.Y., 1980) p. 46.

[5] R.W. Balluffi and L.L. Seigle, Acta Metall., 3 (1955) 170.

[6] D. Hull and D.E. Rimmer, Philos. Mag., 4 (1959) 673.

[7] J.W. Hancock, Met. Sci. J., 10 (1976) 319.

[8] W. Beere and M.V. Speight, Met. Sci. J., 12 (1978) 172.

[9] N.M. Ghoniem, J.N. Alhajji and D. Kaletta, J. Nucl. Mater., 135 (1985) 192.

[10] J.N. Alhajji and N.M. Ghoniem, Acta Metall., submitted.

[11] A.L. Lane and P.J. Goodhew, Philos. Mag. A, 48 (1983) 965.

[12] R.W. Balluffi, in: Interfacial Segregation, Eds. W.C. Johnson and J.M. Blakely (ASM, Metals Park, OH, 1979) p. 193.

[13] W. Bollmann, Crystal Defects and Crystalline Interfaces (Springer-Verlag, Berlin, New York, 1970).

[14] C. Wassilew, in: Proc. Intern. Conf. on Mechanical Behavior and Nucl. Applications of Stainless Steel at Elevated Temperatures, The Metals Society, Varese, Italy, 1981, p. 172.

[15] K.L. Kear and M.H. Wood, "An Analysis of Grain Boundary Failure in Austenitic Stainless Steel," AERE-Harwell Report, AERE-R 10907 (1983).

CONTENTS

[16] W. Beere, Res Mechanica, 2 (1981) 189.

[17] C. Wassilew, W. Kunischaud and B. Ritter, Institute für Material- und Festkörperforschung II, Report KFK PSB-Ber. 2035 (Kl.III), Karlsruhe, West Germany (1981).

[18] K. Herschbach, J. Nucl. Mater., 127 (1985) 239.

COLLISIONAL ASPECTS OF PREFERENTIAL SPUTTERING USING THE MONTE CARLO METHOD

P. S. Chou and N. M. Ghoniem

ABSTRACT

In fusion reactors, surface coatings such as TiC and TiB_2 are susceptible to the influence of preferential sputtering caused by plasma ion bombardment. The preferential sputtering is the result of chemical, diffusional, and kinetic processes. The kinetic processes are dominant at low energy and moderate ion flux.

A Monte Carlo code, TRIPOS, is developed for analysis of the preferential sputtering phenomenon. Argon, helium, deuterium, and tritium ion bombardment of CuFe, CuAu, TiC, and laminated AuPt alloys are simulated. The results from TRIPOS are compared with the results from other theoretical and experimental works. For helium incident on CuAu, TRIPOS gives good agreement with experiment. While TRIPOS shows general agreement with the corresponding program TRIDYD, results for argon on laminated PtAu are not in agreement with EVOLVE. Finally the case of TiC is investigated, where preferential sputtering of carbon atoms under fusion ion bombardment is observed.

Collisional Aspects of Preferential Sputtering Using the Monte Carlo Method*

by

P.S. Chou and N.M. Ghoniem

March 1986

*This work was supported by the National Science Foundation Grant No. CPE-81-11581 and U.S. Department of Energy, Office of Fusion Energy, Grant #DE-FG03-84ER42110, with UCLA

CONTENTS

FIGURES

1. Introduction

Because of the high heat flux on the limiter and the first wall of a fusion reactor, high-Z materials are used for their good thermal conductivities. However, the sputtering erosion of high-Z materials can jeopardize the fusion power balance by inducing excessive radiative energy losses through the introduction of impurities into the plasma. Application of surface coatings such as TiC and TiB_2 to surface components is proposed to mitigate these potential hazards.

In multicomponent materials, it has been observed that surface ion bombardment leads to preferential erosion of one of the constituents. The preferential sputtering phenomenon is not unique to nuclear fusion reactors, but is commonly observed in ion bombardment of alloy surfaces. Earlier investigations on semiconductor materials [1] also indicated this behavior. Recently, this phenomenon has been extensively investigated in experiment and theory. A complete review of experimental work in preferential sputtering is given by Betz and Wehner [2]. However, theoretical progress in this area is hampered by the complexity of the mechnisms controlling preferential sputtering.

The mechanisms for preferential sputtering involve synergistic dynamic, diffusional and microchemical processes. Dynamic processes arise from differences in recoil energy partitioning, implantation and range for different types of bulk atoms in an alloy. Diffusional processes are mainly caused by differences in recoil diffusion, segregation, radiation enhanced diffusion and radiation enhanced segregation for bulk atoms of different types. Microchemical processes originate from local chemical property changes caused by stoichiometric changes such as the changes in surface binding energy, the

formation of new phases, and the implantation of incident ions. The interplay of these three processes obviously complicates the theoretical analysis of preferential sputtering.

It is necessary to isolate each individual mechanism so that a better understanding on this phenomenon can be achieved. This view is reflected in earlier studies such as EVOLVE [3] and TRIDYN [4] which explored the kinetic aspect of preferential sputtering. Such analysis is generally justified under the situation when the energy of the incident ion is low and the ion flux is moderate. The requirement for a moderate ion flux is due to the fact that the ion flux needs to be high enough so as to avoid the domination of the chemical and thermodynamical processes at low flux levels.

The energy partitioning in the kinetic process favors matrix atoms with masses close to those of incident ions. This can be readily seen in the kinetic energy transfer factor, Λ, defined as follows:

$$\Lambda = \frac{4M_1M_2}{(M_1+M_2)^2} \tag{1}$$

where M_1 and M_2 are the masses for incident and recoil atoms, respectively. For identical masses, Λ is 1 and perfect energy coupling is achieved. On the other hand, for a large mass difference, Λ can be close to 0 leading to poor energy coupling. In a fusion reactor, the plasma is mostly composed of deuterium and tritium ions. It is therefore anticipated that light atomic constituents in the first wall and limiters can gain higher recoil energy than the heavier constituents. Furthermore, the interaction cross section for lighter ions is small compared to that of heavier ions. Therefore, lighter recoils can be transported deeper into the surface because of their higher energy and lower interaction cross section. This fact can lead to the depletion of lighter atoms in the surface regions bombarded by fusion ions.

Because of the implantation of incident ions and the recoil mixing effect, the surface composition of an alloy is a function of both ion flux and irradiation time. This renders the analysis for preferential sputtering both time and fluence dependent. The study of the kinetic aspect of preferential sputtering is based on the Monte Carlo code, TRIPOS, developed and used in the earlier chapters [5]. A time dependent option is introduced into the original TRIPOS code. Because of the disagreement in the results from TRIDYN and EVOLVE [4], we investigate the cases of 2 keV Ar on laminated PtAu as in Ref. [3] and 5 keV Ar on LuFe as in Refs. [4] and [6]. We also compare our theoretical work to the experimental results of Nelson and Bastasz [7] for the case of 150 eV ^{3}He on CuAu. Finally, the preferential sputtering effect in TiC coatings caused by fusion ions is investigated.

2. Application of TRIPOS to surface modification problems

The energy losses for ion transport in a solid are caused by nuclear collisions and the interaction with the electron system (electronic stopping). TRIPOS uses continuous power law cross sections to treat the nuclear energy loss and the Biersack-Haggmark electronic stopping [7] to treat the electronic energy loss. Unlike other Monte Carlo code such as TRIM [7], MARLOWE [8], and HERAD [9], the use of the power law cross section in TRIPOS eliminates the need to solve for the time integral for each binary collision. Based on the momentum approximation, the power law cross sections are analytically derived using the power law approximation to the Thomas-Fermi potentials [10,11]. The use of the power law cross section provides a way of estimating the free path between two large-angle collisions, while for the mall angle collisions, the nuclear stopping cross section is used. This scheme allows the free path to be of the order of several lattice constants.

Therefore, TRIPOS bypasses the limitation that the free path be on the order of a lattice constant even though the nuclear energy loss can be negligible.

Because the statistical error associated with analog Monte Carlo decreases with the inverse of particle histories, particle splitting and Russian roulette techniques are used in TRIPOS. The important zone is taken to be the first few atomic layers where most of the sputtered particles originate. A 4 to 1 kill outside this important zone can effectively reduce the computation time by a factor of 3. The analog Monte Carlo method in TRIPOS is a factor of 3-10 faster than the TRIM code. Detailed studies of the relative speed between TRIM and TRIPOS are given in Ref. [12].

The preferential sputtering of an alloy is both time and flux dependent because of the evolution in surface compositions. Therefore, the original TRIPOS code is modified to have time-dependent and composition modification capabilities. There are also other phenomena in preferential sputtering processes requiring further modifications of the TRIPOS code. For example, the recoil implantation and mixing can cause the formation of local super-dense material which leads to local relaxation and expansion. This process is related to the phenomenon of recoil mixing. The super-dense solid is modeled to expand homogeneously until the theoretical density is reached. Because light ions are implanted deeper, such a process can lead to the de-enrichment of heavier atoms in the bulk in a fusion environment.

3. Results of preferential sputtering calculations

The results from TRIPOS simulations of four different cases of preferential sputtering arising from ion bombardment are given as follows.

3.1. Ar on AuPt

In the work by Roush et al., a surface composed of pure gold and platinum layers with a thickness of 40 A altenating was studied. The front surface is gold. The argon ion beam impinges on the surface at an angle of 70 deg with an energy of 2 keV. The surface binding energies are 3.8 eV and 5.9 eV for gold and platinum atoms, respectively. Their results predict a zone of atomic mixing with a depth of about 40 A. However, our calculations using TRIM and the static version of TRIPOS indicate that the projected range for those argon ions is between 14 and 16 A. Also results from dynamic TRIPOS show a 15 A thickness of the mixing zone. This result is not in agreement with the results of EVOLVE. However, it is consistent with the projected range for the incident argon ions. Figure 1 shows plots for relative concentations (represented by pseudo particles) of gold and platinum as functions of pseudo particle histories.

The disagreement between EVOLVE and TRIPOS can be explained by the following argument. Because gold and platinum recoils have very short projected ranges, it is unlikely for argon ions to generate significant recoil implantation-mixing effect at the end of their ranges. The EVOLVE analysis apparently over-estimates the projected range of the argon ions. The sputtering yield from the EVOLVE calculation is larger by a factor of 30% compared to that from TRIPOS. This explains the differences in the surface recession due to sputtering erosion.

3.2. Ar on FeLu

In the investigations conducted by Roush et al. and Moller et al. [4,6], a surface made of 50% iron and 50% lutetium alloy is bombarded with 5 keV argon ions at a normal angle of incidence. The surface binding energy is

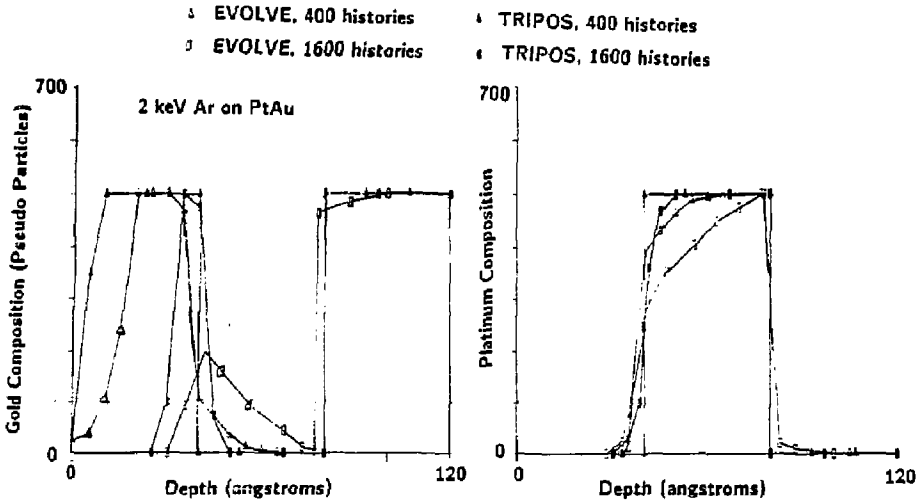

Fig. 1. Composition of gold and platinum as a function of depth predicted from EVOLVE and TRIPOS for 400 and 1600 pseudo particle histories of 2 keV argon ions on laminated PtAu. A pseudo particle history represents a fluence of 5.9×10^{12} ions/cm^2

4.7 eV for both iron and lutetium atoms. The composition profiles from TRIDYN and EVOLVE also show some discrepancies. TRIDYN predicts a depletion of iron atoms below the surface; this depletion zone corespond to the projected range of the argon ion which is 65 Å [4]. For the region beyond the projected range, depletion of lutetium atoms is observed because of iron recoil implantation. For the surface layer, EVOLVE predicts an erichment of iron ions at low fluences and a depletion of iron ions at high fluences. For regions beyond the projected range, an enrichment of lutetium atoms is predicted by EVOLVE for all fluences.

TRIPOS simulation yields results similar to those from TRIDYN as shown in fig. 2. The enrichment of lutetium atoms is below the surface and enrichment of iron atoms around the projected range. Also given in fig. 2 are the results from EVOLVE simulations. Only the enrichment of lutetium is observed over the whole zone. The results from both TRIPOS and TRIDYN strengthen the argument we presented for the previous case of Ar on PtAu. Recoil implantation and mixing of very heavy atoms at the end of range for light incident ions are unlikely to occur, which can be a source of error.

3.3. ^{3}He on CuAu

In the experimental work of Nelson and Bastasz [13], a surface composed of Cu-3%Au is irradiated with 150 eV ^{3}He ions at a normal angle of incidence. The surface binding energies for copper and gold atoms are 3.5 eV and 3.8 eV, respectively. Their results show that the enrichment of gold in the surface increases linearly with the ion fluence with 5%Au at a fluence of 6.0×10^{17} cm^{-2}. Based upon a simplified analytical theory, they concluded that the altered layer, which is the recoil mixing zone, has a thickness

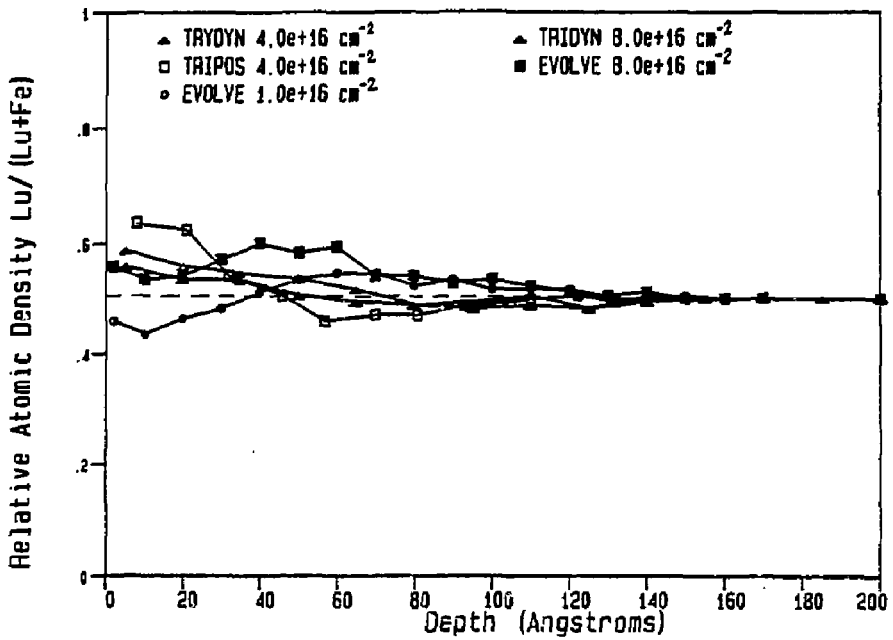

Fig. 2. Relative atomic density of lutetium as a function of depth predicted from EVOLVE, TRIDYN, and TRIPOS for 5 keV argon bombardment of LuFe at different fluences

equal to the projected range of the incident ion. The projected range of 150 ^{3}He ions is about 16 A.

TRIPOS simulation shows an enrichment of gold atoms within a few atomic layers (5-7 A) from the surface. Beyond this region, there is an enrichment of copper atoms from light recoil implantation and mixing up to the end of the projected range. Figure 3 shows that the average enrichment for gold over the projected range agrees well with the experimental results by Nelson and Bastasz [13] for ion fluence up to $4.0 \times 10^{17}/cm^2$. For higher fluences, there is about an 8% difference which is within the experimental error. Another possible cause for this difference can be the formation of a monolayer of gold on the surface which in turn reduces the sputtering of copper atoms. An observation of gold atom enrichment in the first 5-7 A below the surface seems to support this argument.

3.4. Fusion Ions on TiC

The ion considered for this analysis consists of average fusion plasma ions. Because of the presence of the Debye layer in which ions are accelerated to several times their original energy along the surface normal, their angle of incidence is assumed to be normal to the surface and their energy is taken to be a factor of 3 to 5 higher than the average edge plasma temperature. Varga and Taglauer [14] analyzed TiC surfaces bombarded with hydrogen ions with energies in the range of 300 eV and 4 keV. They conclude that there is no measurable surface composition changes in TiC due to the preferential sputtering effect.

The TRIPOS simulations were performed with the surface binding energies of 4.89 eV and 7.47 eV for titanium and carbon atoms, respectively. The energy of incident ions is assumed to be 300 eV. TRIPOS results show that

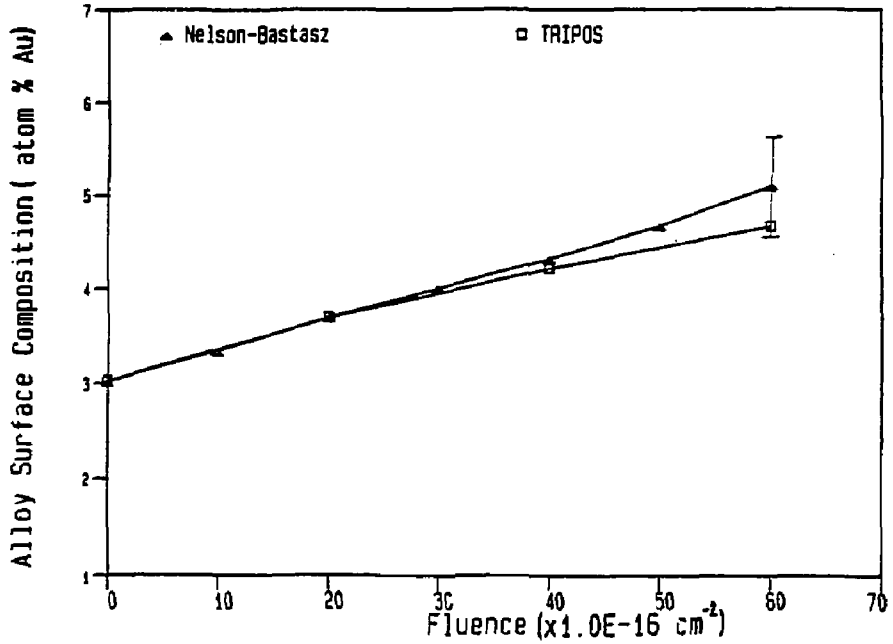

Fig. 3. Gold surface composition in atomic % as a function of fluence resulting from experimental work by Nelson and Bastasz and theoretical calculations from TRIPOS for 150 eV ^{3}He on Cu-3%Au

the sputtering rate for carbon atoms is about twice that for titanium. The projected range is about 80 angstroms. A hundred thousand pseudo particles were used with each representing a fluence of $1x10^{13}/cm^2$. For fluences up to $1x10^{18}/cm^2$, a 50Å thick layer below the surface is enriched with titanium atoms as shown in fig. 4. This result seems not to agree with the experimental observations by Varga and Taglauer. The discrepancy can probably be attributed to the strong influence of microchemical and thermodynamic processes.

4. Conclusions and future directions

The phenomenon of preferential sputtering is an important physical process for fusion reactor and other technological applications. This phenomenon is dominated by the kinetic process at low energy and moderate ion fluence.

A Monte Carlo ion transport code, TRIPOS, is developed for study of the collisional effect on preferential sputtering and surface evolution. This code can simulate the ion bombardment induced composition changes as a function of time and ion fluence. A static version of TRIPOS is more efficient than TRIM which is a static version of TRIDYN. TRIPOS is applied to the preferential sputtering of several alloys under different ion bombardment conditions. The results of TRIPOS on LuFe and CuAu agree with those of TYNDYN as well as with experimental work.

Because of the complex nature of preferential sputtering, theoretical methods seem to fall short of predictions in the case of TiC. Neglecting other preferential sputtering mechanisms seems to result in disagreement between theoretical and experimental results. A comprehensive treatment of preferential sputtering is required to resolve these discrepancies.

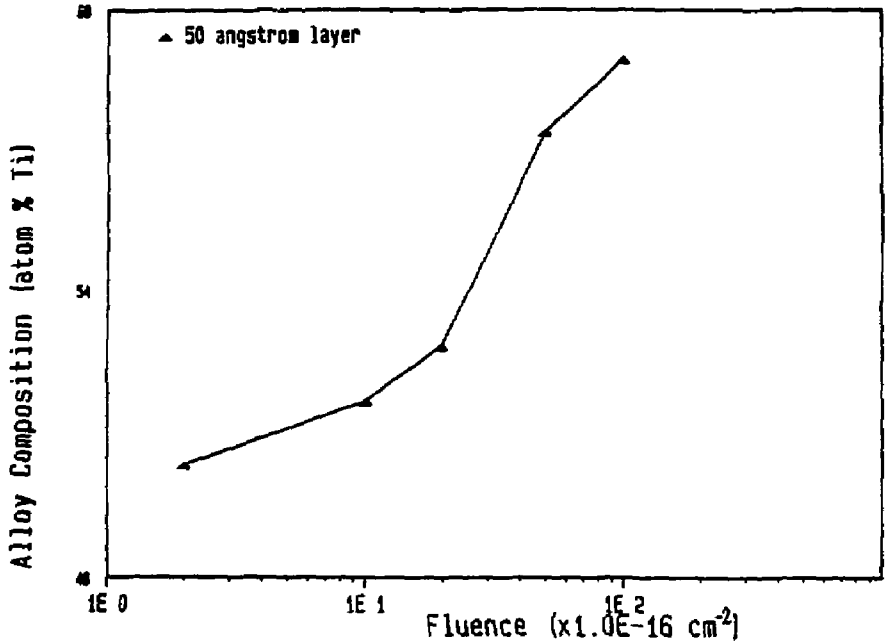

Fig. 4. Titanium surface composition in atomic % as a functic of fluence calculated by TRIPOS for 300 eV fusion ions on a TiC coating

Acknowledgment

This work was supported by the National Science Foundation Grant No. CPE-81-11581 and U.S. Department of Energy, Office of Fusion Energy, Grant No. DE-FG03-84ER42110, with UCLA.

References

1. P.S. Ho, J.E. Lewis, H.S. Wildman, and J.K. Howard, Surf. Sci. 57 (1976) 393.
2. G. Betz and G.K. Wehner, 'Sputtering of Multicomponet Materials' in "Sputtering by Particle Bombardment II", Edt. R. Behrisch, Topics in Applied Physics, Vol. 52, (Springer-Verlag, Berlin, 1983) p. 11.
3. M.L. Roush, T.D. Andreadis, and O.F. Goktepe, Radiat. Eff. 55 (1981) 119.
4. W. Moller and W. Eckstein, Nucl. Instr. Meth. B 2 (1984) 814.
5. P.S. Chou and N.M. Ghoniem, J. Nucl. Mater. 117 (1983) 55.
6. M.L. Roush, F. Davarya, O.F. Goktepe and T.D. Andreadis, Nucl. Instr. Meth. 209/210 (1983) 67.
7. J.P. Biersack and L.G. Haggmark, Nucl. Instr. Meth. 174 (1980) 257.
8. O. Oen and M.T. Robinson, J. Appl. Phys. 35 (1964) 2515.
9. H. Attaya, Ph.D Thesis, University of Wisconsin, UWFDM-420 (1981).
10. J. Lindhard, V. Nielsen, and M. Scharff, Dan. Vid. Selsk. Mat. Fys. Medd. 36 (1968) No. 10.
11. K.B. Winterbon, P. Sigmund, and J.B. Sanders, Dan. Vid. Selsk. Mat. Fys. Medd. 37 (1970) No. 14.
12. P.S. Chou, Ph.D Thesis, UCLA, to be finished in May 1986.
13. G.L. Nelson and R. Bastasz, J. Vac. Sci. Technol. 20 (1982) 498.
14. P. Varga and E. Taglauer, J. Nucl. Mater. 111/112 (1982) 726.

Modeling of Tritium Transport in a Fusion Reactor Pin-Type Breeder Blanket Using the DIFFUSE Code*

by

Rodger Martin and Nasr M. Ghoniem

March 1986

*This work was supported by the U.S. Department of Energy, Office of Fusion Energy, Grant #DE-FG03-80ER52061, with UCLA.

CONTENTS

FIGURES

Abstract

Modeling of Tritium Transport in a Fusion Reactor
Pin-Type Solid Breeder Blanket Using the DIFFUSE Code

Rodger Martin and Nasr M. Ghoniem

A pin-type fusion reactor blanket is designed using γ-$LiAlO_2$ solid tritium breeder. Tritium transport and diffusive inventory are modeled using the DIFFUSE code. Two approaches are used to obtain characteristic $LiAlO_2$ grain temperatures. DIFFUSE provides intragranular diffusive inventories which scale up to blanket size. These results compare well with a numerical analysis, giving a steady-state blanket inventory of 13 g.

Start-up transient inventories are modeled using DIFFUSE for both full and restricted coolant flow. Full flow gives rapid inventory buildup while restricted flow prevents this buildup. Inventories after shutdown are modeled: reduced cooling is found to have little effect on removing tritium, but preheating rapidly purges inventory.

DIFFUSE provides parametric modeling of solid breeder density, radiation, and surface effects. 100% dense pins are found to give massive inventory and marginal tritium release. Only large trapping energies and concentrations significantly increase inventory. Diatomic surface recombination is only significant at high temperatures.

1. Introduction

The present fusion reactor blanket design uses γ-$LiAlO_2$ for tritium breeding due to high temperature structural stability. Bulk diffusive tritium inventory is based on the diffusivity, which for γ-$LiAlO_2$ from 400 to 700°C is given by an activation energy of 35.8 kcal/mol/°K and a pre-exponential term of 1.2×10^{-6} cm^2/s [1].

STARFIRE [2] first attempted tritium transport modeling in solid breeders with a percolation model to approximate tritium oxide partial pressures over $LiAlO_2$. The BCSS [3] and FINESSE [4] models begin with the analytical solution for diffusion in a single spherical grain with zero surface concentration; intragranular diffusive inventory is given by:

$$I_g = [\ r_g^2 / 15\ D\ ]\ \dot{g}\ V_g\ . \qquad (1)$$

with $\dot{g}$ the tritium generation rate, V_g the grain volume, and r_g the grain radius. From blanket temperature and tritium generation profiles, the intragranular inventories are calculated and scaled up to represent unit cells, and then summed to give total blanket diffusive inventory.

Other contributions to inventory arise from solubility, grain boundary diffusion, surface adsorption, and purge gas inventory. Reactor inventory includes tritium permeation into the coolant and metal structure. All models consider grain boundary, adsorptive, and purge inventories negligible compared to diffusive. Solubility inventory is also negligible for $LiAlO_2$. The TRIO experimental results support these conclusions [1].

Although useful, the previous models do not address the following:
(1) all models employ exponential approximations, not actual blanket temperature and generation profiles;
(2) modeling of transient operation is limited;

(3) the analytical solution presupposes zero concentration on spherical grain surfaces;

(4) limited experimental data and no models exist of irradiation effects;

(5) large variations exist in reported diffusion coefficients;

(6) oxidation/reduction effects on purged tritium are poorly understood.

This research attempts to address the first four areas.

2. Modeling tritium transport in a pin-type blanket

The present modeling uses the DIFFUSE code [5] for a one-dimensional numerical solution of the diffusion equation. This code is useful for modeling tritium generation, inventory, and release in solid breeders as well as permeation.

Fick's laws govern the DIFFUSE analysis:

$$J_j(x,t) = -D_j(T(x,t)) \left[\nabla C_j(x,t) + \frac{C_j(x,t)\, Q^*}{kT^2(x,t)} \nabla T(x,t) \right] \qquad (2)$$

and

$$\partial C_j(x,t)/\partial t = -\nabla J_j(x,t) + G_j(x) - \sum_i \partial C_T{}^{ij}(x,t)/\partial t \ , \qquad (3)$$

where the concentrations $C_j(x,t)$ and $C_T{}^{ij}(x,t)$ represent the j^{th} diffusing species and the j^{th} species in the i^{th} trap respectively, $G_j(x)$ the implant (generation) source term, $J_j(x,t)$ the flux, $D_j(T)$ the diffusivity, Q^* the heat of transport, k Boltzmann's constant, and $T(x,t)$ the temperature. Solutions can be obtained for slab, spherical, or cylindrical geometries. Appropriate choice of source terms simulates tritium generation.

DIFFUSE can evaluate several boundary conditions:

(1) perfectly reflecting boundary (e.g. impermeable oxide layer);

(2) zero concentration at the boundary;

(3) Sievert's law (bulk solubility);

(4) diatomic surface recombination;

(5) simple interface between two materials.

As in previous models, bulk diffusion is assumed to dominate inventory in $LiAlO_2$. Given the tritium generation rate and a representative cell temperature, a characteristic grain can be used to model each unit cell. Use of the zero concentration boundary condition by the DIFFUSE code gives the intragranular diffusive inventories which are scaled up to give the total blanket inventory. Detailed neutronics analysis provides tritium generation and volumetric heating rates.

The temperature chosen for each characteristic grain is important; two approaches are used for evaluation. The first divides each pin into five concentric zones of equal thickness. The temperature for the volumetrically averaged radial position of each zone is determined from the heat transfer profiles. Each zone is represented by one grain at this temperature and the pin generation rate. DIFFUSE gives the diffusive inventory for this grain, which is scaled up for the zone and the five zones summed for the pin inventory. This analysis is performed for a pin from each row, and extrapolated to blanket dimensions.

The second method, evaluation of pin inventory from a single DIFFUSE analysis, requires a characteristic single grain temperature representative of the entire rod inventory. Manipulation of equation 1 gives another equation amenable to numerical analysis:

$$\bar{T} = Q \,/\, R \ln \left[\frac{2}{r_o^2 - r_i^2} \int_{r_i}^{r_o} \exp\,(Q/RT)\; r\; dr \right] . \qquad (4)$$

Substitution of $T = T(r)$ gives $\bar{T}$ for the single DIFFUSE analysis.

A third method employs a derivative form of equation 1 to numerically evaluate the diffusive inventory for each characteristic grain at an average pin temperature weighted by diffusive inventory. The working equation is:

$$\bar{I}_g = \frac{2\, r_g^2\, \dot{g}}{15\, D_o\, (r_o^2 - r_i^2)} \int_{r_i}^{r_o} \exp\,(Q/RT)\; r\; dr \qquad (5)$$

which only requires the temperature profile $T = T(r)$ obtained from thermal hydraulics. D_o and Q are the pre-exponential and activation energy terms for diffusion, and r_i and r_o the inner and outer radii of the ceramic within the pin.

3. Steady-state inventory

Figure 1 shows a module from this blanket design. Each $LiAlO_2$ pin has a central channel for the helium purge and a 0.1 mm gap between the ceramic and 1 mm thick 9-C cladding. Behind the lobular first wall are six rows of 1.7 cm diameter beryllium pins for neutron multiplication. Next are five rows of $LiAlO_2$ pins of purge channel radius 0.05 cm and outer radius 0.61 cm, then six rows of larger pins of radii 0.135 and 1.46 cm. Helium coolant flows past the first wall and through the module at 50 atm pressure, with inlet and outlet temperatures of 250 and 550°C. The cladding has an oxide layer to reduce tritium permeation. The maximum $LiAlO_2$ temperature approaches 1150°C and the minimum 530°C. The $LiAlO_2$ grain size is 0.1 μ, and overall ceramic density is set at 85% of maximum for greater porosity and faster tritium release.

The 5-zone approach for steady-state diffusive inventory gives 12.9 g of tritium. The method of one DIFFUSE analysis per pin gives 12.6 g. The

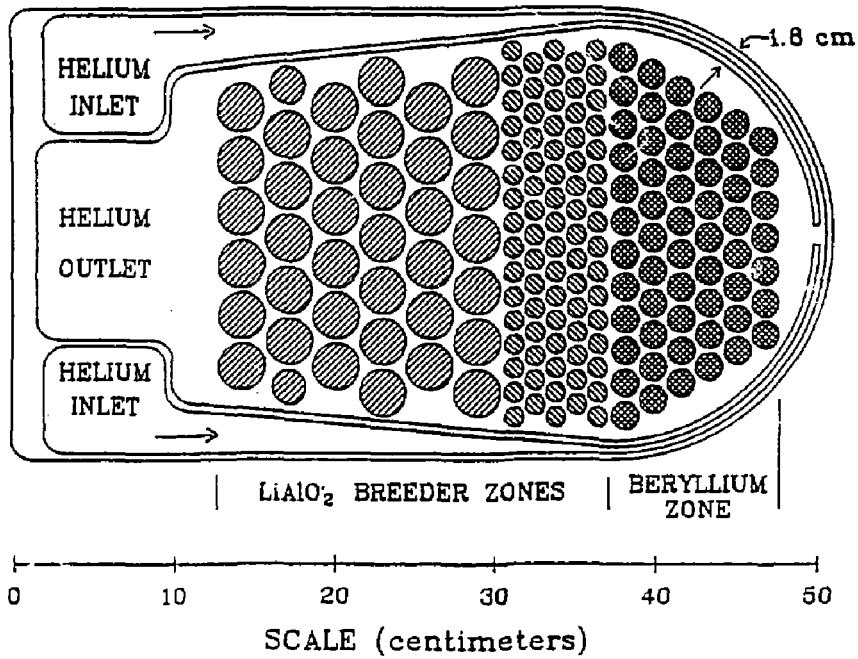

Fig. 1. Design of blanket module

numerical evaluation gives 13.2 g. These methods show very good agreement. Inventory of 0.10 wppm in this 129,000 kg $LiAlO_2$ blanket compares favorably with the GA Technologies model results of 38.3 g inventory (0.073 wppm) in a 522,000 kg $LiAlO_2$ blanket [6].

Figure 2 gives row-by-row inventories. The high first row temperatures reduce inventory to 0.03 wppm; likewise for rows six through eleven with less than 0.02 wppm. The cooler pins of rows two through five have inventories approaching 0.6 wppm.

With the diffusive tritium inventory only 13 grams at steady-state, the major concern might be high temperature permeation through pin cladding. With an inner oxide layer on the cladding to resist permeation, these concerns are assumed manageable and are not quantified.

4. Transient tritium inventory

Two different start-up conditions are modeled: helium coolant flow through the blanket at 100% that of full power operation, and reduced helium flow. For each, a two week start-up is modeled with 3.5 days each at 10%, 20%, 50%, and 80% followed by 100% power.

With 100% helium flow, the fractional tritium generation and volumetric heating rates and the coolant temperature rise across the blanket are the same as the fractional power level. New temperature profiles across the pins are calculated and equation 5 gives the temperature representative of each row for each power level. A sequence of five DIFFUSE runs for a single grain gives transient inventories at each power characteristic of the row.

With fractional helium flow restricted to the same fraction as the power level at 20%, 50%, and 80%, coolant temperature rise across the blanket is identical to full power operation, giving significantly higher transient

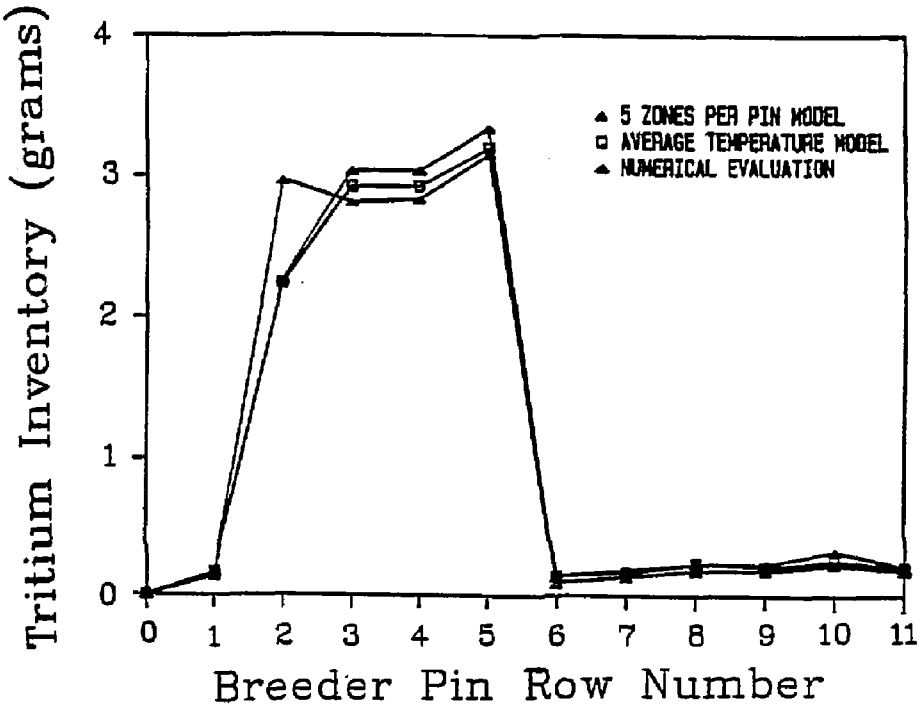

Fig. 2. Comparison of steady-state tritium inventory modules

temperatures. For 10% power, helium flow is maintained at 20% of maximum, so coolant temperature rise across the blanket is only half that of full power.

Figure 3 shows that full flow inventory builds up rapidly to several hundred grams at low power before decreasing rapidly at higher power. The first row contributes most to inventory with its high generation rates. For restricted flow the colder temperatures at 10% power give some tritium build-up, but inventory decreases rapidly at 20% power.

Significant inventory will accumulate for unrestricted helium flow during start-up. Tailoring of helium flow to power alleviates these concerns. Even controlled flow gives some inventory build-up at low power testing and start-up, but coolant pre-heating would alleviate such concerns.

Two shutdown scenarios are evaluated: coolant flow at 20% that of full power, and a combination of coolant flow reduction and preheating for coolant temperatures of 470 to 500°C across the pins. Zero tritium generation and afterheat generation of 1% that at full power are assumed.

For the first scenario the temperature rise from inlet to each row of pins is 1/20 that of full power. New pin temperature profiles and characteristic temperatures are calculated. Steady-state conditions for each grain are followed by a second DIFFUSE run using temperature and generation profiles at shutdown.

Figure 4 shows the cold shutdown scenario to give negligible reduction of inventory with time. From a steady-state inventory of 12.6 g, 12.4 g remains after two weeks, 12.1 g after 6 months, and 11.7 g after one year. With ceramic temperatures near 270°C blanket inventory will be virtually immobilized after shutdown.

In comparison, average temperatures for hot shutdown range over 200°

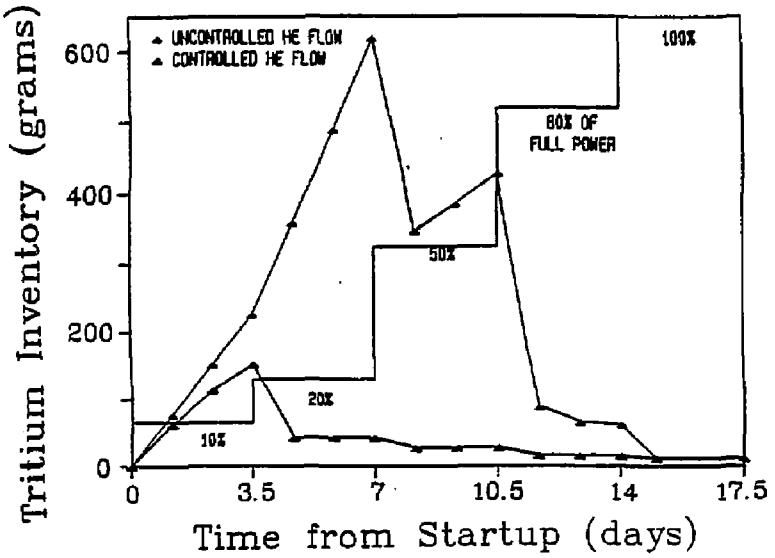

Fig. 3. Blanket inventory during start-up transients

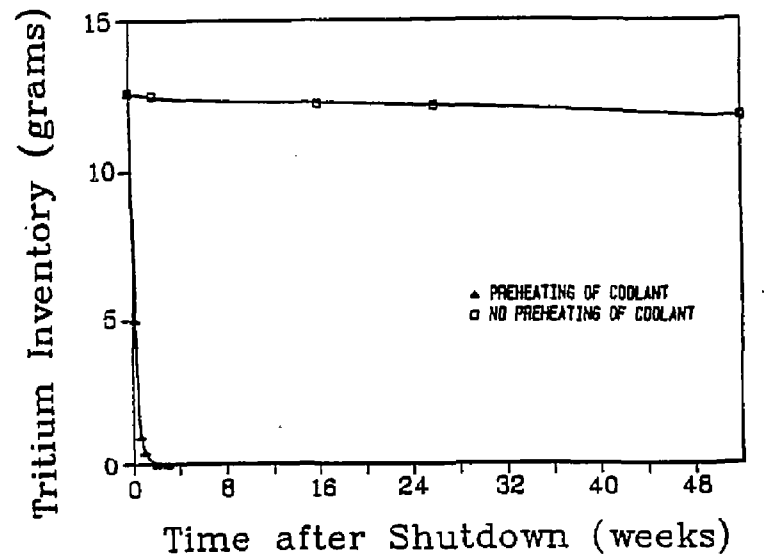

Fig. 4. Blanket inventory after shutdown

higher with much faster diffusion. One week after shutdown, total blanket inventory drops from 12.6 to 0.45 g, and after two weeks a trivial 0.02 g remains. With coolant pre-heating, purge of diffusive inventory can be considered complete within days.

For this small inventory, the expense of coolant preheating may not be worth the benefits obtained. But if larger blanket inventory results from actual operations, blanket baking could rapidly alleviate post-shutdown inventory concerns.

5. Effects of solid breeder properties

DIFFUSE is used to study effects on inventory of three solid breeder physical properties: density, surface effects, and radiation effects [7,8].

DIFFUSE analyzes density effects for this pin design using 100% dense $LiAlO_2$. Tritium diffusion is evaluated in a massive single-grain cylinder with zero concentration boundary condition at the purge channel and reflecting boundary condition (oxide layer) at the cladding. The temperature profiles calculated previously give very slow tritium diffusion through these massive grains. Over three years only 1.7% of the total generated tritium is purged from the hottest pins; the cooler pins release only a few hundredth of a percent. Huge inventories are a significant safety concern. Advantages are the possibility of batch processing of pins for tritium recovery at the end of blanket life, reduced permeation problems, and enhanced tritium breeding ratio from higher density.

Surface effects are evaluated using the diatomic surface recombination boundary condition for a typical $LiAlO_2$ grain. With the lack of experimental data, input values for surface properties felt to be reasonable are used. Results indicate negligible surface inventory with respect to diffusive over

low to medium temperatures. Measurable surface contribution to the total inventory only becomes apparent above 1100°K; the contribution at 1400°K is 65% that of diffusive, although uncertainties in input values make quantitative analysis very tentative.

Radiation effects are approximated using combinations of temperature, radiation-produced trap concentration, and trapping energy. Experimental uncertainties lead to use of input values which seem reasonable. For a trap concentration of one appm in $LiAlO_2$, the trapped inventory is overwhelmed by diffusive over a reasonable range of trapping energies. At 1273°K the trapped inventory is comparable to diffusive only at a large trap energy of 4 eV. For an assumed trap energy of 3.5 eV and a temperature of 1273°K, the trapped inventory is comparable only at trap concentrations of 100 appm and more. Assuming a very large trap concentration of 1% atomic fraction, a comparison of inventories from 700 to 1475°K is made for trap energies of 2.5 and 3.5 eV: at 3.5 eV the trapped inventory is overwhelming while at 2.5 eV the trapped inventory is predominant at low temperatures but rapidly becomes insignificant at temperatures much above 825°K. These results suggest significant trapping requires trapping energies above 3 eV, and that effects due to low trap concentration are only significant at high temperatures while very high trap concentrations have most significance at lower temperatures.

6. Conclusions

(1) The total diffusive steady-state tritium inventory for this blanket is expected to be 13 g.

(2) For start-up power ramping, unrestricted coolant flow will rapidly lead to hundreds of grams of tritium inventory. Reduction of coolant flow can keep inventory at acceptable levels.

(3) Restricted coolant flow after shutdown will not significantly affect the residual inventories. Preheating of the coolant can lead to rapid purging.
(4) Use of 100% dense $LiAlO_2$ will lead to massive inventories over blanket life, but the marginal release rates would favorably impact permeation concerns. Post-shutdown batch processing may be feasible.
(5) At low to moderate breeder temperatures, diffusive inventory is expected to predominate. Considerable radiation-induced trap concentrations and trapping energies would be required for predominance of trapped inventory.
(6) The *DIFFUSE* code offers much potential in modeling tritium behavior in solid breeders under a wide range of operating conditions and phenomena.

Acknowledgements

Support by a University of California Los Angeles Chancellor's Fellowship is gratefully acknowledged. The support of Department of Energy, Grant #DE-FG03-80ER52061 to UCLA is appreciated.

References

1. R. G. Clemmer et al., "The TRIO Experiment", Argonne National Laboratory Report ANL-84-55 (1984).
2. C. C. Baker et al., "STARFIRE - A Commercial Tokamak Fusion Power Plant Study", Argonne National Laboratory Report ANL/FPP-80-1 (1980), p. 10-94.
3. M. Abdou et al., "Blanket Comparison and Selection Study - Final Report", Argonne National Laboratory Report ANL/FPP-84-1 (1984).
4. M. Abdou et al., "FINESSE: A Study of the Issues, Experiments and Facilities for Fusion Nuclear Technology Research and Development", Interim Report, Vol. 3, PPG-821/UCLA-ENG-84-30 (1984).
5. M. I. Baskes, "DIFFUSE 83", SAND-83-8231 (1983).
6. M. Abdou et al., "Blanket Comparison and Selection Study", ibid., p. 8-147.
7. R. Martin and N. M. Ghoniem, "Modeling of Tritium Transport in a Pin-Type Solid Breeder Blanket", PPG-934/UCLA-ENG-8608 (1986).
8. R. Martin, "Effects of Radiation Damage on Tritium Diffusion in Fusion Solid Breeders", unpublished manuscript.